Gyroid versus double-diamond in ABC triblock copolymer melts

M. W. Matsen
Polymer Science Centre, University of Reading, Whiteknights, Reading RG6 6AF, United Kingdom

(Received 31 July 1997; accepted 30 September 1997)

Monodisperse melts of ABC linear triblock copolymer are examined using self-consistent field theory (SCFT). Our study is restricted to symmetric triblocks, where the A and C blocks are equal in size and the A/B and B/C interactions are identical. Furthermore, we focus on the regime where B forms the majority domain. This system has been studied earlier using density functional theory (DFT), strong-segregation theory (SST), and Monte Carlo (MC), and it corresponds closely to a series of isoprene–styrene–vinylpyridine triblocks examined by Mogi and co-workers. In agreement with these previous studies, we find stable lamellar, complex, cylindrical, and spherical phases. In the spherical phase, the minority A and C domains alternate on a body-centered cubic lattice. In order to produce alternating A and C domains in the cylinder phase, the melt chooses a tetragonal packing rather than the usual hexagonal one. This amplifies the packing frustration in the cylinder phase, which results in a large complex phase region. Contrary to the previous evidence that the complex phase is double-diamond, we predict the gyroid morphology. The earlier theoretical results are easily rationalized and the experimental data are, in fact, more consistent with gyroid. © *1998 American Institute of Physics.* [S0021-9606(98)50602-2]

I. INTRODUCTION

Block copolymer molecules provide superb systems for studying phenomena related to molecular self-assembly. Typically, researchers choose to work with the AB diblock architecture because it is the simplest and best understood.[1–3] To a good approximation, its phase behavior depends on only three quantities, χN, f, and a_A/a_B[4], where χ is the Flory–Huggins interaction parameter between A and B segments, N is the total degree of polymerization, f specifies the composition of the diblock, a_A is the A segment length, and a_B is the B segment length. At this point, experiment[5–7] and theory[8] agree on the equilibrium diblock copolymer phases: lamellae (L), gyroid (G), hexagonally packed cylinders (C_h), and body-center cubic spheres (S_{bcc}). Mean-field theory also predicts an ordered phase of weakly bound close-packed spheres (S_{cp}) in a narrow region along the order–disorder transition (ODT).[8,9] However, fluctuations presumably destroy the long-range order, creating a region of randomly close-packed spheres in the disordered phase consistent with experiment.[10] Note that experiment[5] and theory[8] also agree on the existence of a highly metastable perforated-lamellar (PL) phase in the region where G is stable.

Many have been intrigued by the bicontinuous cubic morphology first observed in 1976 by Aggarwal.[11] In 1986, Thomas *et al.*[12] provided evidence that it was a double-diamond structure consisting of two interweaving fourfold coordinated lattices. More recently in 1994, a similar bicontinuous structure with two threefold coordinated lattices was identified and denoted as the gyroid phase.[6] Afterward, concerns were raised over the possible confusion between double-diamond and gyroid when identifying morphologies by transmission electron microscopy (TEM). It was suggested that a definitive phase assignment also required small-angle x-ray scattering (SAXS) or small-angle neutron scattering (SANS), which can distinguish between double-diamond and gyroid based on their space-group symmetries, $Pn3m$ and $Ia3d$, respectively. Using SAXS, a reexamination of numerous samples previously identified as double-diamond revealed their true morphology to be gyroid.[7] Evidently, the double-diamond phase does not occur in diblock melts because it produces a large degree of packing frustration.[1,2]

In general, changing the architecture of an AB block copolymer does not alter the topology of the phase diagram from that of the simple diblock system.[13] Perhaps it might reverse the relative stability of the gyroid and perforated-lamellar phases,[4] but we anticipate nothing more. After all, the physics involved in microphase separation[1,2] remains essentially the same except for a few minor issues.[14] To produce a significant change in behavior requires something else, such as a third component, i.e., ABC block copolymers.

The linear ABC triblock represents a model system for examining the phase behavior of three-component block copolymers. It can be described by seven quantities: three interaction parameters, two volume fractions to specify the composition, and two ratios to provide the relative segment lengths. Naturally, the microphase separation of these molecules will in general be more complicated than for diblocks, because it is possible to have three distinct interfaces instead of just one, and there are stretching energy contributions from three distinct blocks rather than just two. Stadler *et al.*[15,16] have experimentally examined numerous triblock molecules and have cataloged a number of new morphologies. On the theoretical side, Zheng and Wang[17] have used density functional theory (DFT)[18] to examine 11 different structures over a large parameter range. Nevertheless, these studies only scratch the surface because the parameter space is so vast. Even if we limit our attention to conformationally symmetric segments (i.e., $a \equiv a_A = a_B = a_C$), there are still five parameters to consider. To make things manageable, we

focus on the reduced parameter space of symmetric triblocks where the two endblocks have the same volume fraction (i.e., $f \equiv f_A = f_C$) and equivalent interactions with the midblock (i.e., $\chi \equiv \chi_{AB} = \chi_{BC}$). This symmetric system needs just three parameters, f, χN, and χ_{AC}/χ, to describe it, and often the latter parameter is virtually irrelevant.[19]

The symmetric ABC triblock system has been studied experimentally by Mogi and co-workers,[20–23] and theoretically by Nakazawa and Ohta[19] using DFT. These results are in good agreement. As the B block increases in size, the morphology evolves from lamellar to double-diamond, to cylindrical, to spherical. The cylinders pack tetragonally with alternating A and C domains, and the spheres pack on a body-centered cubic lattice again with alternating A and C domains. In the complex phase, the A and C domains each form a diamond lattice embedded in a B matrix, and because the two lattices are distinct, its space-group symmetry is $Fd3m$. It should be noted that neither of these studies considered the possibility that the complex phase could be gyroid with two distinct threefold lattices and a space-group symmetry $I4_132$. Although recent Monte Carlo simulations[24] support the double-diamond morphology, we should be cautious in accepting this experimental phase assignment[20–22] in light of the numerous gyroid samples previously misidentified as double-diamond.[7] This concern is further justified by recent calculations of Phan and Fredrickson[25] that suggest a preference for gyroid over double-diamond using strong-segregation theory (SST).[26]

Below, we apply self-consistent field theory (SCFT)[27] to the system of symmetric ABC triblock melts. Our study examines the portion of the phase diagram where B forms the majority component and focuses on the relative stability of gyroid and double-diamond. Just as in the simpler diblock system, we find a strong preference for the gyroid phase. The earlier theoretical evidence for double-diamond[19,24] is easily explained and the experimental data[20–22] are in fact more consistent with gyroid.

II. THEORY

In this section, we outline the self-consistent field theory (SCFT)[27] for a melt of n identical ABC linear triblock copolymers, where the A, B, and C blocks consist of $f_A N$, $f_B N$, and $f_C N$ segments, respectively ($f_A + f_B + f_C = 1$). The segments are assumed to be incompressible and are defined based on a common volume, $1/\rho_0$. Hence, the total volume of the melt is $\mathscr{V} = nN/\rho_0$. The SCFT used here assumes completely flexible Gaussian A, B, and C segments with statistical lengths, a_A, a_B, and a_C, respectively. The internal energy U of the melt is approximated by

$$\frac{U}{nk_BT} = \frac{N}{\mathscr{V}}\int [\chi_{AB}\phi_A(\mathbf{r})\phi_B(\mathbf{r}) + \chi_{BC}\phi_B(\mathbf{r})\phi_C(\mathbf{r}) + \chi_{AC}\phi_A(\mathbf{r})\phi_C(\mathbf{r})]d\mathbf{r}, \tag{1}$$

where χ_{AB}, χ_{BC}, and χ_{AC} are the usual Flory–Huggins interaction parameters, and $\phi_\alpha(\mathbf{r})$ is a dimensionless density of α segments. Because of the incompressibility assumption,

$$\phi_A(\mathbf{r}) + \phi_B(\mathbf{r}) + \phi_C(\mathbf{r}) = 1. \tag{2}$$

To examine periodic microstructures, we implement the Fourier method developed in Ref. 28, where a complete derivation is provided for the diblock system. Because the extension to an ABC triblock melt is straightforward, we just outline the algorithm for calculating its free energy. The first step involves generating a set of basis functions $f_i(\mathbf{r})$ to represent each spatially dependent quantity [i.e., $\phi_A(\mathbf{r}) = \Sigma_i \phi_{A,i} f_i(\mathbf{r})$]. The functions $f_i(\mathbf{r})$ are chosen so that they possess the symmetry of the microstructure being considered, so that they are eigenfunctions of the Laplacian operator [i.e., $\nabla^2 f_i(\mathbf{r}) = -\lambda_i D^{-2} f_i(\mathbf{r})$], and so that they are orthonormal [i.e., $\mathscr{V}^{-1}\int f_i(\mathbf{r}) f_j(\mathbf{r}) d\mathbf{r} = \delta_{ij}$]. They are indexed by $i = 1, 2, 3, \ldots$, and ordered such that their eigenvalues λ_i form a nondecreasing series. In all cases, the series begins with the identity function, $f_1(\mathbf{r}) = 1$. Given the space-group symmetry of the microstructure, the remaining basis functions can be looked up in Ref. 29. For the tricontinuous gyroid (G) phase, the first few basis functions are

$$f_2(\mathbf{r}) = \sqrt{4/3}[\sin(X)\cos(Y) + \sin(Y)\cos(Z) + \sin(Z)\cos(X)], \tag{3}$$

$$f_3(\mathbf{r}) = \sqrt{8/3}[\cos(X)\sin(Y)\sin(2Z) + \cos(Y)\sin(Z)\sin(2X)) + \cos(Z)\sin(X)\sin(2Y)], \tag{4}$$

$$f_4(\mathbf{r}) = \sqrt{4/3}[\cos(2X)\cos(2Y) + \cos(2Y)\cos(2Z) + \cos(2Z)\cos(2X)], \tag{5}$$

where $X = 2\pi x/D$ is a dimensionless length, Y and Z are defined similarly, and D is the size of the unit cell. For the tricontinuous double-diamond (D) phase,

$$f_2(\mathbf{r}) = 2[\cos(X)\cos(Y)\cos(Z) + \sin(X)\sin(Y)\sin(Z)], \tag{6}$$

$$f_3(\mathbf{r}) = \sqrt{4/3}[\cos(2X)\cos(2Y) + \cos(2Y)\cos(2Z) + \cos(2Z)\cos(2X)], \tag{7}$$

$$f_4(\mathbf{r}) = \sqrt{4/3}[\cos(3X)\cos(Y)\cos(Z) + \cos(X)\cos(3Y)\cos(Z) + \cos(X)\cos(Y)\cos(3Z) - \sin(3X)\sin(Y)\cos(Z) - \sin(X)\sin(3Y)\sin(Z) - \sin(X)\sin(Y)\sin(3Z)]. \tag{8}$$

All we require from the basis functions are the eigenvalues λ_i and the coefficients,

$$\Gamma_{ijk} = \frac{1}{\mathscr{V}}\int f_i(\mathbf{r}) f_j(\mathbf{r}) f_k(\mathbf{r}) d\mathbf{r}. \tag{9}$$

Because the basis functions form an infinite series, they have to be truncated in order to perform a calculation. We keep enough so that the numerical inaccuracy is smaller than the resolution of our plots, i.e., the linewidths. In some cases, this required up to 400 functions.

In SCFT, molecular interactions are replaced by mean fields $w_\alpha(\mathbf{r})$, which act on the α segments. To perform a SCFT calculation, we have to evaluate the segment densities

$\phi_\alpha(\mathbf{r})$ for a melt of noninteracting triblocks subjected to these fields. This is done by calculating the symmetric matrix,

$$A_{ij} = -\tfrac{1}{6} N a_A^2 \lambda_i D^{-2} \delta_{ij} - \sum_k w_{A,k} \Gamma_{ijk}, \tag{10}$$

and from that a transfer matrix $T_A(s) \equiv \exp(As) = U_A D_A U_A^T$, where U_A is a unitary matrix containing the eigenvectors of A, and D_A is a diagonal matrix with elements $\exp(\epsilon_{A,i} s)$ where $\epsilon_{A,i}$ are the eigenvalues of A. Similarly, transfer matrices, $T_B(s)$ and $T_C(s)$, are constructed for the B and C blocks, respectively.

In terms of the transfer matrices, Fourier coefficients of two end-segment distribution functions are evaluated:

$$q_i(s) = \begin{cases} T_{A,i1}(s), & \text{if} \quad 0 < s < f_A, \\ \sum_j T_{B,ij}(s - f_A) T_{A,j1}(f_A), & \\ \quad \text{if} \quad f_A < s < 1 - f_C, & \\ \sum_{jk} T_{C,ij}(s - 1 + f_C) T_{B,jk}(f_B) T_{A,k1}(f_A), & \\ \quad \text{if} \quad 1 - f_C < s < 1, & \end{cases} \tag{11}$$

and

$$q_i^\dagger(s) = \begin{cases} \sum_{jk} T_{A,ij}(f_A - s) T_{B,jk}(f_B) T_{C,k1}(f_C), & \\ \quad \text{if} \quad 0 < s < f_A, & \\ \sum_j T_{B,ij}(1 - f_C - s) T_{C,j1}(f_C), & \\ \quad \text{if} \quad f_A < s < 1 - f_C, & \\ T_{C,i1}(1 - s), \quad \text{if} \quad 1 - f_C < s < 1. & \end{cases} \tag{12}$$

From them, the Fourier coefficients for the segment densities are evaluated. Those for the A-segment distribution $\phi_A(\mathbf{r})$ are given by

$$\phi_{A,i} = \frac{1}{q_1(1)} \int_0^{f_A} ds \sum_{jk} q_j(s) q_k^\dagger(s) \Gamma_{ijk}. \tag{13}$$

Expressions for the B- and C-segment distributions differ only in their intervals of integration. These integrals can all be evaluated analytically in terms of the above eigenvalues and eigenvectors, which are functions of the fields.

The fields and the densities calculated from them must satisfy self-consistent field equations,

$$w_{A,i} - w_{B,i} + \chi_{AB} N (\phi_{A,i} - \phi_{B,i}) - (\chi_{AC} N - \chi_{BC} N) \phi_{C,i} = 0, \tag{14}$$

$$w_{C,i} - w_{B,i} + \chi_{BC} N (\phi_{C,i} - \phi_{B,i}) - (\chi_{AC} N - \chi_{AB} N) \phi_{A,i} = 0, \tag{15}$$

$$\phi_{A,i} + \phi_{B,i} + \phi_{C,i} = 0, \tag{16}$$

where $i = 2,3,4\ldots$. (We are free to set $w_{A,1} = \chi_{AB} N f_B + \chi_{AC} N f_B$, $w_{B,1} = \chi_{AB} N f_A + \chi_{BC} N f_C$, and $w_{C,1} = \chi_{BC} N f_B + \chi_{AC} N f_A$.) The solution for a particular phase and set of parameters can be found by making a reasonable initial guess (usually a nearby solution) followed by a quasi-Newton iteration method.[30]

Once the field equations are solved, the free energy F of the phase is evaluated using

$$\frac{F}{n k_B T} = -\ln[q_1(1)] - \sum_i (\chi_{AB} N \phi_{A,i} \phi_{B,i} + \chi_{BC} N \phi_{B,i} \phi_{C,i} + \chi_{AC} N \phi_{A,i} \phi_{C,i}). \tag{17}$$

For each ordered periodic phase, the free energy has to be minimized with respect to the lattice size D, and for the disordered state, the free energy simplifies to $F/n k_B T = \chi_{AB} N f_A f_B + \chi_{BC} N f_B f_C + \chi_{AC} N f_A f_C$. Comparing the free energies of the different phases allows us to construct a phase diagram. Furthermore, the free energy calculations provide other relevant quantities such as domain sizes and segment distributions.

III. RESULTS

A good understanding of the ABC triblock behavior can be achieved by examining the reduced parameter space corresponding to symmetrical endblocks where $f \equiv f_A = f_C$ and $\chi \equiv \chi_{AB} = \chi_{BC}$, and conformationally symmetric segments where $a \equiv a_A = a_B = a_C$. This class of ABC triblocks is characterized by just three quantities, f, χN, and χ_{AC}/χ. Below, we examine the interval $0 \leqslant f \leqslant 0.3$, where the center block forms the majority domain. In this region, the stable structures have no internal A/C interfaces, and consequently χ_{AC}/χ generally has little influence on phase behavior; so for now, we fix $\chi_{AC}/\chi = 1$.

Just as with diblock melts, the composition of the triblock f tends to control the geometry of the ordered microstructure and χN mainly affects the degree of segregation. To illustrate the effect of χN, we plot three profiles of a $f = 1/4$ lamellar phase. At this composition, the melt is weakly segregated below $\chi N \sim 21$. Weak segregation often implies that the single-harmonic approximation[31] is sufficient to represent segment profiles, but that is not true in this case because the period of the B domains is half that of the A and C domains. Figure 1(b) shows the profile at $\chi N = 50$, which is well into the intermediate-segregation regime. At this degree of segregation, the concentration in each domain reaches about 0.99. If we choose to define strong segregation as the regime where these concentrations exceed 0.9999, then the crossover to strong segregation occurs near $\chi N \sim 100$, which corresponds to Fig. 1(c). Note that strong-segregation theories (SST) are not necessarily accurate for $\chi N \gtrsim 100$ since they also assume strongly stretched chains, which require χN to be much larger.[32]

Figure 1 demonstrates a reduction in interfacial width and a growth in domain spacing with increasing segregation. In Fig. 2, the domain spacing D is plotted logarithmically as a function of segregation χN. For $\chi N \gtrsim 200$, the spacing approximately scales as $D \sim a \chi^{1/6} N^{2/3}$, consistent with the dashed line calculated using SST (see Sec. IV). Both the strong-segregation scaling[23,33] and the departure from it at

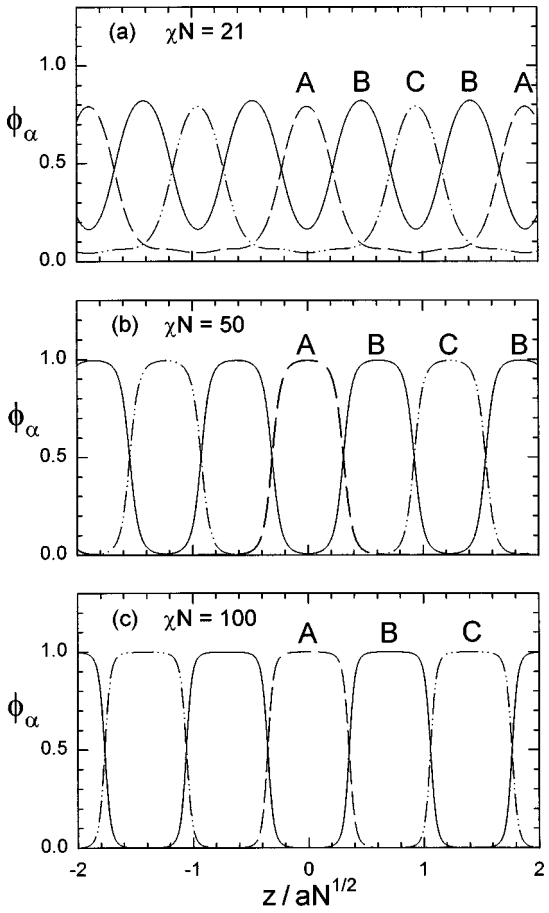

FIG. 1. Profiles of a lamellar phase formed by a symmetric ABC triblock with $f=0.25$ and $\chi_{AC}/\chi=1$. In each plot, the A-, B-, and C-segment densities are represented by dashed, solid, and dash-dotted curves, respectively. The first profile (a) at $\chi N=21$ is near the crossover from weak to intermediate segregation, the second (b) at $\chi N=50$ is in the intermediate-segregation regime, and the third (c) at $\chi N=100$ is near the crossover from intermediate to strong segregation.

intermediate segregations are analogous to those of the diblock system.[8] Naturally, this dependence of domain size on segregation is general to all the triblock microstructures. In Fig. 3, we fix the segregation at $\chi N=50$ and plot the

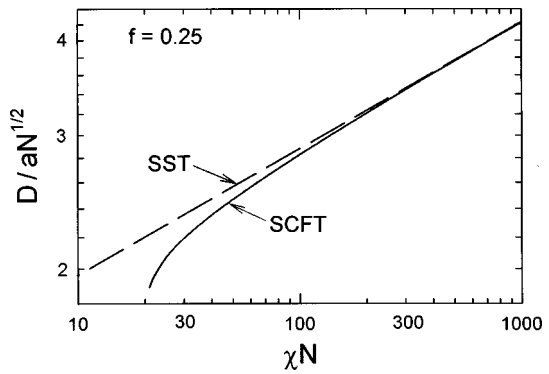

FIG. 2. Period of the lamellar phase D plotted logarithmically as a function of segregation χN for a symmetric triblock with $f=0.25$ and $\chi_{AC}/\chi=1$. The solid curve is obtained using SCFT and the dashed curve corresponds to the SST expression in Eq. (22).

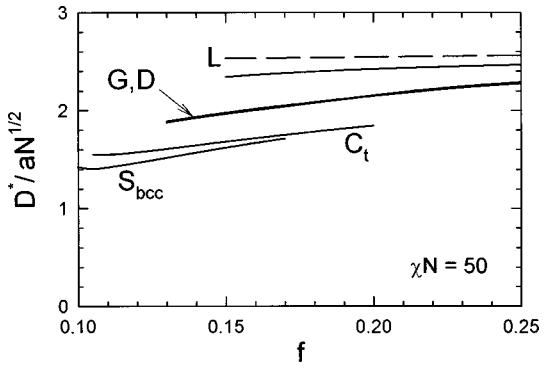

FIG. 3. Characteristic domain size, $D^*=2\pi/q^*$, where q^* is the principal scattering vector, plotted as a function of composition f with $\chi N=50$ and $\chi_{AC}/\chi=1$. The solid curves for the lamellar (L), cylinder (C_t), spherical (S_{bcc}), gyroid (G), and double-diamond (D) phases are calculated with SCFT. The dashed curve represents the SST expression in Eq. (22) for the L phase.

domain size as a function of composition f. To compare the different geometrical structures, we characterize their domain sizes by $D^*\equiv 2\pi/q^*$, where q^* is the magnitude of the principal scattering vector. For both lamellae (L) and tetragonal cylinders (C_t), D^* is the size of their respective unit cells. For the spherical (S_{bcc}), gyroid (G), and double-diamond (D) phases, $D^*=D$, $D/\sqrt{2}$, and $D/\sqrt{3}$, respectively, where D is the dimension of their cubic unit cells. Evidently, we can anticipate discontinuities in D^* or q^* on the order of 15% at the various order–order transitions (OOTs).

Figure 3 makes no statement regarding which phases are stable and where the different OOTs occur. This is determined from Fig. 4, where their free energies are plotted as a function of f, again with $\chi N=50$. The sequence of stable phases is disordered $\rightarrow S_{bcc}\rightarrow C_t\rightarrow G\rightarrow L$, and the transitions between them occur at $f=0.101$, 0.121, 0.145, and 0.198.

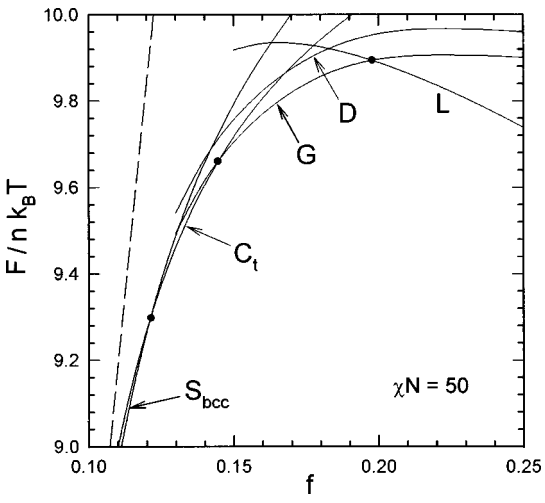

FIG. 4. Free energies F for the lamellar (L), cylinder (C_t), spherical (S_{bcc}), gyroid (G), double-diamond (D), and disordered phases as a function of composition f with $\chi N=50$ and $\chi_{AC}/\chi=1$. The free energy of the disordered state is shown with a dashed curve, and phase transitions are denoted by dots.

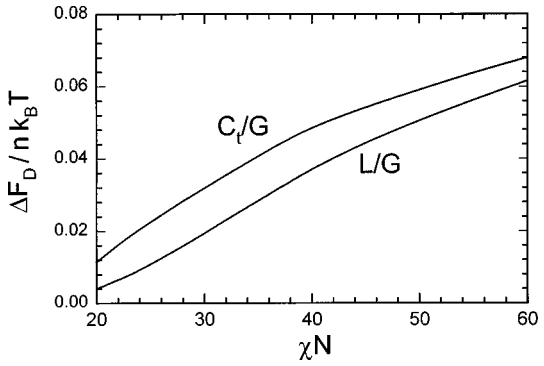

FIG. 5. Excess free energy ΔF_D of the double-diamond (D) phase plotted as a function of segregation χN along the L/G and C_t/G phase boundaries with $\chi_{AC}/\chi = 1$.

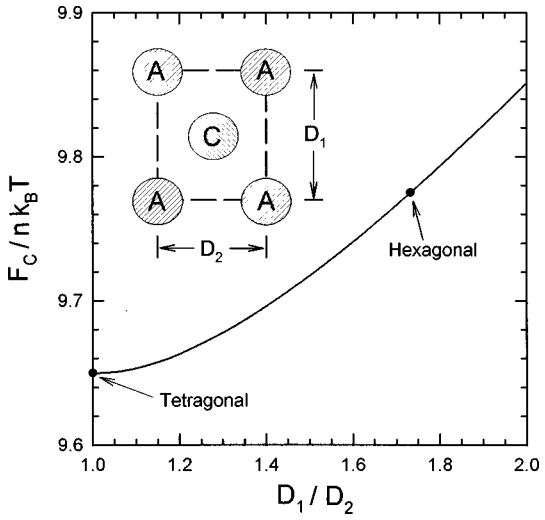

FIG. 6. Free energy F_C of the cylinder phase at $f = 0.1438$, $\chi N = 50$, and $\chi_{AC}/\chi = 1$ plotted against the aspect ratio D_1/D_2 of its unit cell. The tetragonal (square) packing of cylinders corresponds to $D_1/D_2 = 1$ and the hexagonal (triangular) packing occurs at $D_1/D_2 = 3^{1/2}$.

The locations of these OOTs differ significantly from previous experimental[20–22] and theoretical[17,19] estimates, and we will provide sensible explanations for this. The far more serious concern is that we predict the complex phase to be gyroid while Refs. 19–22 all suggest double-diamond.

Although D is much less stable than G in Fig. 3, it is conceivable that D may become stable as the segregation is changed. To check this possibility, Fig. 5 plots the excess free energy ΔF_D of the double-diamond phase along the C_t/G and L/G phase boundaries as a function of χN. Along each boundary, ΔF_D remains positive and hence double-diamond remains unstable. Furthermore, the monotonic increase in ΔF_D suggests that D remains unstable up to the strong-segregation limit, which is strongly supported by SST calculations in Ref. 25 and by simple explanations provided in Sec. VI.

So far, we have accepted the theoretical[19,25] and experimental[20–22] evidence that cylinders pack tetragonally, but this preference is not obvious. In the diblock system, it is natural for cylinders to pack hexagonally because this fills space well, but in ABC triblock melts there is an additional consideration. The A- and C-rich cylinders must be placed close together because the B blocks have to bridge between them. On average, it is only possible to have four A cylinders neighboring each C cylinder, and vice versa. This is accomplished with the $D_1 \times D_2$ rectangular unit cell shown in Fig. 6, where a C cylinder is placed in the body-centered position and A cylinders are placed at the four corners. Tetragonal packing corresponds to $D_1/D_2 = 1$. Although this arrangement of cylinders does not fill space well, it does distribute the A cylinders uniformly around the C cylinder. Hexagonal packing occurs when $D_1/D_2 = \sqrt{3}$. While this is the ideal arrangement for filling space, it distributes the A cylinders asymmetrically about the C cylinder. It is hard to know without calculating the free energy F_C shown in Fig. 6 that the tetragonal packing is most favored. Evidently, the hexagonal packing is not even metastable, i.e., it does not even represent a local minimum in the free energy.

The body-centered cubic (bcc) lattice of spheres is best able to fill space without producing large gaps,[34] and therefore it is the arrangement generally selected by the diblock system. It is also suitable for triblock melts, because it allows the A- and C-type spheres to alternate in a CsCl-type arrangement so that all nearest-neighbor pairs have opposite compositions. Near the order–disorder transition (ODT), we have to consider the possibility of other arrangements. Because the A and C blocks are short, they can easily pull free from their domains, swelling the matrix and reducing packing frustration. This is reflected by a small increase in D^* (see Fig. 3), which is also observed for diblock melts.[1,4] In the diblock system, the reduced packing frustration allows spheres to reorder into a close-packed configuration,[8,9] but that should be prevented here because neither the face-center cubic (fcc) nor the hexagonally close-packed (hcp) lattice allows the spheres to be arranged with all nearest-neighbor pairs having opposite compositions. This is consistent with calculations by Nakazawa and Ohta[19] using DFT, and by Phan and Fredrickson[25] using SST. Note that when the symmetry between A and C is broken, other arrangements, such as simple cubic (i.e., NaCl-type packing), may become stable.

With reasonable confidence that the stable phases have been identified, we calculate the phase diagram shown in Fig. 7. At large f, other morphologies consisting of minority B domains embedded in an A/C lamellar matrix have been observed.[15] For the moment, we ignore them since previous calculations[15,17] indicate that they are well outside the range of our phase diagram. Even with 400 basis functions, we can only calculate the boundaries of the gyroid phase accurately up to $\chi N \sim 65$; the dotted lines beyond that are simple extrapolations. The gyroid phase shows no clear sign of pinching off at strong segregations as it does in the diblock system;[8] nevertheless, we expect it to, based on SST calculations by Phan and Fredrickson.[25] There are only a couple of qualitative differences between this triblock phase diagram and the diblock one.[8] Here, there is no narrow region of close-packed spheres near the ODT, and the S_{bcc} phase pinches off at weak segregations, producing the triple point

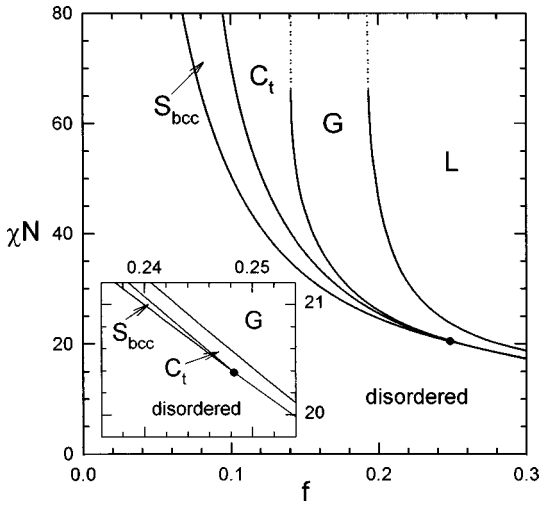

FIG. 7. Phase diagram for symmetric ABC linear triblocks plotted as a function of composition f and segregation χN with $\chi_{AC}/\chi=1$. The symbols L, G, C_t, and S_{bcc} denote lamellae, gyroid, tetragonal cylinders, and body-centered cubic spheres. All the phase transitions are discontinuous, and the dotted curves are extrapolated phase boundaries. The inset magnifies the region around a triple point indicated by the dot.

at $f=0.248$ and $\chi N=20.38$ (see the inset of Fig. 7).

So far, we have only considered $\chi_{AC}/\chi=1$, a value sufficient to produce segregation between the A and C blocks. To assess its effect on phase behavior, Fig. 8 shows the phase diagram as a function of χ_{AC}/χ and f, with $\chi N=50$. The ordered phases near the top of the diagram all have well segregated A and C domains. As χ_{AC}/χ is lowered, the A and C blocks begin to mix, and eventually a transition occurs to a phase in which the endblocks are completely mixed. A transition of this nature has been observed by Neumann *et al.*[35] Here, we distinguish the phases using primed symbols to denote those with completely mixed endblocks. The boundaries between the primed and unprimed phases behave as expected; as the endblocks become smaller, larger values of χ_{AC}/χ are necessary to produce A/C segregation. Note that the L/L′, G/G′, and S_{bcc}/S'_{bcc} transitions are all continuous, but the C_t/C'_h transition is discontinuous because it involves a rearrangement of cylinders from tetragonal to hexagonal. Also notice that a close-packed spherical (S'_{cp}) phase occurs along the ODT when the A and C blocks are mixed, but not when they are segregated.

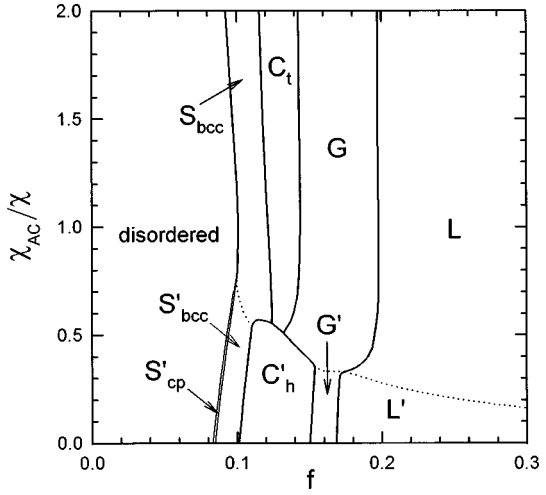

FIG. 8. Phase diagram for symmetric ABC linear triblocks plotted as a function of composition f and the ratio χ_{AC}/χ with $\chi N=50$. The symbols, L, G, C_t, C_h, S_{bcc}, and S_{cp}, represent lamellae, gyroid, tetragonal cylinders, hexagonal cylinders, body-centered cubic spheres, and close-packed spheres, respectively. Primed symbols denote phases in which the A and C blocks are completely mixed. Solid curves correspond to discontinuous transitions and dotted curves represent continuous transitions. Note that the $\chi_{AC}/\chi=0$ limit corresponds to the ABA triblock system.

As we have claimed, the χ_{AC} interaction parameter generally has little influence on phase behavior once the A and C blocks are segregated. This is because none of the L, G, C_t, and S_{Abcc} phases possess any A/C interfaces, and thus their free energies are nearly independent of χ_{AC}. So naturally, the OOTs between them in Fig. 8 are almost vertical. However, the free energy of the disordered phase, $F/nk_BT=2\chi f(1-2f)+\chi_{AC}f^2$, clearly depends on χ_{AC}, and so the ODT should shift to smaller f with increasing χ_{AC}; it does, but only slightly. This is partly because the ODT occurs at small f, and also because the segregation in the S_{bcc} phase drops off significantly near the ODT, producing a similar χ_{AC} dependence in its free energy that tends to cancel with that of the disordered state to produce a relatively vertical ODT.

IV. COMPARISON WITH OTHER THEORIES

The strong-segregation theory (SST) developed by Semenov[26] is believed to provide the $\chi N\to\infty$ limit of SCFT, although there is some evidence that it might not.[36] Even though SST does not accurately represent experiments, which are performed at finite segregations, it has the advantage that it produces simple analytic expressions. For the lamellar phase, SST predicts the entropic stretching energy to be[33]

$$\frac{F_{el}}{nk_BT}=\left[\frac{\pi^2 f_A}{32a_A^2}+\frac{3f_B}{8a_B^2}+\frac{\pi^2 f_C}{32a_C^2}\right]\frac{D^2}{N},\equiv\alpha\frac{D^2}{N}. \tag{18}$$

The coefficient for the B-block stretching energy differs from the other two because both ends of the B block are constrained to the interface, while the A and C blocks each have a free end. This fact was neglected in Ref. 23. The interfacial energy is given by[37]

$$\frac{F_{int}}{nk_BT}=2\left[g_{AB}\left(\frac{\chi_{AB}N}{6}\right)^{1/6}+g_{BC}\left(\frac{\chi_{BC}N}{6}\right)^{1/6}\right]\frac{N^{1/2}}{D},$$
$$\equiv\beta\frac{N^{1/2}}{D}, \tag{19}$$

where

$$g_{AB}\equiv\frac{a_A+a_B}{2}\left[1+\tfrac{1}{3}\left(\frac{a_A-a_B}{a_A+a_B}\right)^2\right], \tag{20}$$

and g_{BC} is given by an analogous expression. Minimizing the total free energy, $F=F_{el}+F_{int}$, with respect to D, provides the equilibrium domain spacing,

$$\frac{D}{N^{1/2}}=\left(\frac{\beta}{2\alpha}\right)^2. \tag{21}$$

For symmetric triblocks with $f\equiv f_A=f_C$, $\chi\equiv\chi_{AB}=\chi_{BC}$, and $a\equiv a_A=a_B=a_C$, this expression reduces to

$$\frac{D}{aN^{1/2}}=2\left(\frac{8\chi N}{3[6+(\pi^2-12)f]^2}\right)^{1/6}, \tag{22}$$

which compares well with our SCFT results in Figs. 2 and 3. Just as in the diblock system,[8] SST estimates the domain spacings far better than one should expect given the level of approximations involved.[38] Other quantities are generally predicted far less accurately.[1,32]

Lyatskaya and Birshtein[39] have used SST to examine three different morphologies, which include the L and C_t phases examined here. They locate the C_t/L boundary at $f=0.18$. This estimate will be somewhat inaccurate because of a need to supplement SST with various approximations when dealing with nonlamellar structures.[36] Stadler *et al.*[15] have examined more complicated phases and have used rather crude approximations to obtain analytic expressions, which we suspect has led to qualitatively incorrect predictions.[40] This underscores the importance of employing the more advanced numerical techniques.[41] Doing so, Phan and Fredrickson[25] have illustrated a preference for gyroid over double-diamond, but neither structure is stable in the strong-segregation limit. The stable phases in their study are S_{bcc}, C_t, and L, with the S_{bcc}/C_t and C_t/L transitions located at $f=0.048$ and 0.155, respectively. Although these SST values are consistent with our SCFT calculations, they too will contain some degree of inaccuracy due to approximations involving the chain trajectories and the shape of the internal interfaces. With the most recent advances by Likhtman and Semenov,[42] it is now possible to avoid such approximations.

There are several ABC triblock calculations that implement the density functional theory (DFT) of Ohta and Kawasaki.[18] SCFT and DFT both apply mean-field theory to the same standard Gaussian model, but DFT makes a number of additional approximations. Previous comparisons have shown that these approximations cause large inaccuracies in the DFT,[8,36] and this is also evident in the ABC triblock calculations. DFT predicts the C_t/S_{bcc} and L/C_t transitions to approach $f=0.14$ and 0.28, respectively, as $\chi N\to\infty$.[17,19] These values differ enormously from those of SST,[25] and furthermore they greatly exceed any reasonable extrapolation of our SCFT results in Fig. 7. Perhaps more serious is the fact that DFT predicts a huge interval, $0.17\lesssim f\lesssim 0.34$, at $\chi N=\infty$, where double-diamond is supposedly more stable than L and C_t.[19] Although we find such an interval, it is much smaller ($0.168\leqslant f\leqslant 0.183$ at $\chi N=50$ and $0.167\leqslant f\leqslant 0.176$ at $\chi N=70$) and seems to disappear by $\chi N\sim 100$, consistent with the SST results of Phan and Fredrickson.[25] Reference 19 admits that when their DFT calculation is applied to the diblock system, double-diamond wipes out the entire lamellar region, which is a very disturbing result!

The weak-segregation theory (WST) of Leibler,[31] which is the small χN approximation to SCFT, has not yet been used to estimate phase boundaries in the triblock system. However, Werner and Fredrickson[43] have used it to calculate the disordered state structure functions, and from that the spinodal lines indicating where the disordered state becomes unstable to harmonic fluctuations. In the diblock system, the spinodal line is a good indicator of the order–disorder transition (ODT), but we doubt that is the case in the triblock system since the single-harmonic approximation is no longer reliable. We attribute their unusual behavior associated with the L/L' transition in Fig. 8 to the failure of the single-harmonic approximation. In general, it will be necessary to retain numerous harmonics[44] even at weak segregations, and this will make Leibler-type calculations very involved. Considering that such calculations are only applicable in a narrow region along the ODT, they are surely not worth the effort unless fluctuation corrections[44,45] are of interest.

Recently, Dotera and Hatano[24] examined symmetric ABC linear triblocks using a Monte Carlo method, and at a composition of $f=0.233$, their simulation produced a double-diamond microstructure. Although that seems to contradict our prediction that gyroid is highly preferred, there are many possible explanations. First of all, their simulation is performed on very short molecules only 30 segments in length. Certainly, the entropic stretching energy of the individual blocks will not be Gaussian as we have assumed. Second, their model constrains polymers to a lattice. Because the lattice constant is not significantly smaller than the domain size of the microstructure, the lattice could produce unphysical effects. Third, just as with experiments, Monte Carlo simulations are susceptible to nonequilibrium effects, which can leave the system trapped in a metastable state. Fourth, their small simulation box, which contains just one unit cell of the D phase, will result in finite-size effects. The most serious is likely the constraint it imposes on the period of the microstructure. Dotera and Hatano have examined box sizes of L=36, 40, 44, and 50, and only in the L=40 case did the double-diamond phase result. Assuming this roughly corresponds to the equilibrium size of its unit cell, we could expect the G phase at L≈33, 66, 99,..., none of which were examined in their study. The fact the simulation box size has a strong effect on stability makes it virtually impossible to determine the equilibrium phase. Nevertheless, Monte Carlo simulations could play an important role in identifying new morphologies, which then could be tested for stability by SCFT calculations.

V. COMPARISON WITH EXPERIMENT

Mogi and co-workers[20–23] have examined a series of isoprene–styrene–vinylpyridine (ISP) triblock copolymers with endblocks of approximately equal size. Because the I/S and S/P interactions are similar, these molecules closely approximate the symmetric triblocks examined in our theoretical study. As the volume fraction f of the endblocks is increased, the experiments find a transition from body-center cubic spheres (S_{bcc}) to tetragonal cylinders (C_t) near

$f \sim 0.115$, followed by a transition to a tricontinuous complex phase near $f \sim 0.165$, and then to lamellae (L) at around $f \sim 0.275$. The structure of the classical phases, L, C_t, and S_{bcc}, and the sequence in which they occur, agree well with our theoretical predictions. For the moment, we ignore the fact experiments identified the complex phase as double-diamond (D) while SCFT predicts gyroid (G).

It is difficult to quantitatively compare the experimental phase boundaries to those in Fig. 7. The small experimental deviations from $f_A = f_C$, $\chi_{AB} = \chi_{BC}$, and $a_A = a_B = a_C$ will affect the phase boundaries to some degree, but we could account for this in our SCFT calculation. However, we cannot account for the nonequilibrium effects. Lipic *et al.*[46] have illustrated that it can be extremely difficult, if not impossible, to anneal out metastable states even at only intermediate degrees of segregation. As a result, the phases observed in experiment will typically correspond to values of χN much lower than the actual ones. This is because ordered samples are typically produced starting in the disordered state and increasing segregation by either lowering temperature or solvent casting. Increasing χN can slow the kinetics sufficiently to prevent the order–order transitions (OOTs). Even prolonged annealing afterward for weeks, months, or years may be unable to induce the equilibrium state. These effects can easily account for the differences between the experimental and theoretical phase boundaries.

The one glaring inconsistency between experiment and theory is the complex phase assignment. Using both small-angle x-ray scattering (SAXS) and transmission electron microscopy (TEM), Mogi *et al.*[20–22] concluded the complex phase was double-diamond, whereas we predict gyroid. This could be attributed to nonequilibrium effects associated with solvent casting. Naturally, solvent will reduce packing frustration, which may stabilize the double-diamond phase.[47] Although the sample should switch to gyroid as the solvent evaporates, this could be prevented by slow kinetics. Nevertheless, we will demonstrate that the more likely explanation was an experimental misidentification of the phase. This has happened on numerous other occasions,[7] and furthermore Mogi *et al.* never considered gyroid as a possible candidate.

Interpreting SAXS measurements from ABC copolymers is more difficult than from AB copolymers. In the latter case, the relative electron densities between domains only affects the scattering contrast, but in the ABC system, they also affect the relative scattering intensities. To interpret their scattering data, Mogi *et al.*[22] have assumed that $\Delta\rho_I \approx -\Delta\rho_P$, where $\Delta\rho_I \equiv \rho_I - \rho_S$ is the difference in electron densities between the I and S domains and $\Delta\rho_P \equiv \rho_P - \rho_S$ is the difference between the P and S domains. Based on this assumption, a number of reflections will be nearly extinguished, which for the lamellar phase will include all the even reflections. For the cylinder phase, we can expect to lose the [110], [200], [220], [310],... reflections, leaving just the [100], [210], [300], [320],... peaks. As for the spherical phase, [110], [200], [211], [220],... should be nearly extinguished, leaving only [100], [111], [210], [221], [300],... The experimental scattering patterns for the cylindrical and spherical phases are consistent with these predictions, but the lamellar phase clearly exhibits even reflections, contrary to the assumption $\Delta\rho_I \approx -\Delta\rho_P$.

Their typical SAXS patterns from the complex phase did not exhibit any scattering peaks. Incorrectly, Mogi *et al.*[22] claimed this to be consistent with the double-diamond structure and the assumption $\Delta\rho_I \approx -\Delta\rho_P$.[48] In reality, only [220], [222], [400], [422],... should be extinguished, leaving reflections at [111], [311], [331], [333], [511],... and according to SCFT, the [111] peak will be strongest followed by [311] at about 24% the intensity. As for the G phase, [211], [220], [400],... should be nearly extinguished, leaving us with [110], [310], [222], [321], [330],... of which [110] should be strongest, followed by [310] at about 32% the intensity. Previously, SCFT has predicted scattering intensities in good agreement with experiment.[8] The absence of scattering peaks may simply be a result of insufficient long-range order. Lowering the segregation should improve the order and indeed their low-molecular-weight sample did exhibit peaks, which they labeled as [220], [400], and [422] in support of double-diamond. However, we strongly disagree with this assignment. First of all, those are the peaks that should be nearly extinguished. Second, the relatively large width of the [400] peak suggests it is really two unresolved peaks. Third, the principal [111] reflection, which should be the strongest, is not even observed. Fourth, the principal scattering vector has an exceptionally small magnitude, which is highly unexpected (see Fig. 3), especially considering that it was measured from a low-molecular-weight sample. Ideally, Mogi *et al.* would have confirmed that this magnitude was consistent with the dimensions in the TEM images, but they did not. At any rate, we are unable to rationalize the scattering patterns in terms of either the G or D structures. This might be because the sample contained traces of a second kinetically trapped phase.

The experimental TEM images of the complex phase are of good quality and provide the best evidence to its actual structure. They can be directly compared to the SCFT since it predicts all the segment distributions. In Fig. 9, we show simulated TEM images for the [111] direction, which is the threefold symmetry axis. The images on the left are both generated for the G phase, and the two on the right are for the D phase. The top images correspond to samples stained with OsO_4, which turns the I, S, and P domains black, white, and gray, respectively, and the bottom two images represent PTA, which just stains the P domains black. Images 9(a) and 9(b) should be compared to Fig. 2(b) in Ref. 20, Figs. 1(a) and 4(d) in Ref. 21, and Fig. 2(c) in Ref. 22, while images 9(c) and 9(d) should be compared to Fig. 2(d) in Ref. 22. In all cases, our G simulations compare very well to the experimental images, while the D ones are much less successful. Mogi and co-workers also observed images with fourfold symmetry presumably from the [100] direction. Although this direction only has a twofold symmetry axis, samples with an appropriate thickness can produce fourfold symmetry. Figures 10(a) and 10(b) simulate TEM images of the G and D phases stained with OsO_4. Again, the experimental images, shown in Figs. 5(d) and 6(a) of Ref. 21, agree much better with the simulated image of G.

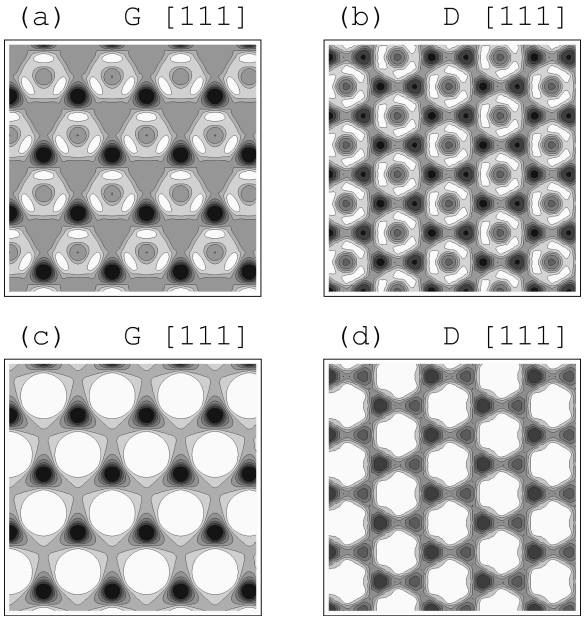

FIG. 9. Simulated TEM images of the gyroid (G) and double-diamond (D) structures generated at $f=0.25$, $\chi N=50$, and $\chi_{AC}/\chi=1$ from slices cut orthogonal to the [111] direction. In the (a) and (b) images, the contrast is proportional to $\phi_B(\mathbf{r})/2+\phi_C(\mathbf{r})$ integrated along the direction of the electron beam, and in (c) and (d), the contrast is proportional to the integral of $\phi_C(\mathbf{r})$. The sample thickness T for the G phase is a complete repeat period ($T/aN^{1/2}=2.81$), and for the D phase it is a third of a period ($T/aN^{1/2}=2.28$) located at $D/4\leqslant x+y+z\leqslant 5D/4$, where D is the unit-cell dimension. Each image is $3D\times 3D$ in size, where $D/aN^{1/2}=3.24$ and 3.95 for the G and D phases, respectively.

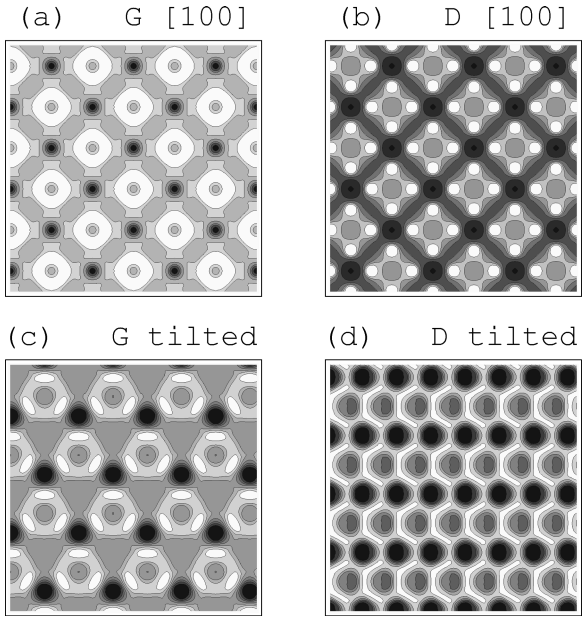

FIG. 10. Simulated TEM images of the gyroid (G) and double-diamond (D) structures generated at $f=0.25$, $\chi N=50$, and $\chi_{AC}/\chi=1$ from slices cut orthogonal to the [100] direction. In all four cases, the contrast is proportional to the integral of $\phi_B(\mathbf{r})/2+\phi_C(\mathbf{r})$. In the (a) and (b) images, the segment densities are integrated along the [100] direction, and in (c) and (d), they are integrated along the [111] direction to simulate a tilt of 57.4°. The sample thickness T is a complete repeat period ($T/aN^{1/2}=3.24$) for the G phase, and half a period ($T/aN^{1/2}=1.97$) for the D phase located at $0\leqslant x\leqslant D/2$, where D is the unit-cell dimension. Each image is $3D\times 3D$ in size.

A TEM simulation requires us to choose a sample thickness and its position relative to the unit cell. The fact that Mogi *et al.*[21,22] reported their published images to be typical strongly suggests that their samples contain approximately one repeat period of the microstructure. All samples of this special thickness will produce identical images, whereas in general, the sample position causes significant variations in the image. Therefore, we simulated all our TEM images of the G phase using a full repeat period. However, doing the same for the D phase produces images with no resemblance to the experiment, contrary to arguments by Mogi *et al.*[21] To produce double-diamond images with some resemblance requires us to select particular fractions of a repeat period with very specific positions in the unit cell. Consequently, our simulated images of the D phase cannot be considered typical.

To confirm the orientational relation between TEM images with threefold and fourfold symmetry, Mogi *et al.*[21] performed a tilt experiment. They tilted their samples associated with the [100] direction 54.7° to reorient them presumably in the [111] direction. As they expected, this transformed the fourfold symmetry into the threefold symmetry. All this seems to suggest is that the complex phase is cubic, which is consistent with both the G and D structures. However, it suggests more than that because the tilting experiment will transform a [100] image into a [111] image only if the sample thickness is a complete repeat period. This is illustrated in Figs. 10(c) and 10(d), where we simulate a 54.7° tilt of the images in Figs. 10(a) and 10(b). Clearly, the double-diamond phase is not capable of explaining the tilt experiment, but the gyroid phase is.

The $\chi_{AC}=0$ limit, corresponding to symmetric ABA triblocks, has recently been examined independently by Laurer *et al.*[49] and by Avgeropoulos *et al.*[50] using styrene–isoprene–styrene triblock copolymers. At a composition of $f=0.16$, both studies identified the gyroid morphology, which agrees perfectly with the G′ phase in Fig. 8. In both the ABA and ABC systems, the B blocks have both ends effectively constrained to the interfaces. The only real difference is that B blocks are prevented from forming looped configurations[14] in the ABC system. This will definitely affect the free energies of gyroid and double-diamond, but presumably in the same way since the structures are so similar. The important difference between G and D is the amount of packing frustration in their minority domains,[2] which has nothing to do with the B domain. So if the ABA system prefers gyroid, then so should the ABC system, which further strengthens our speculation that Mogi *et al.*[20–22] misidentified the complex phase.

Matsushita *et al.*[51] also present evidence for a tricontinuous double-diamond structure, but for a styrene–isoprene–vinylpyridine triblock at $f\approx 0.17$. This is similar to the triblocks used by Mogi *et al.* except that the styrene and isoprene blocks have been swapped. Because this causes a significant asymmetry in the A/B and B/C interfacial tensions,[17] our phase diagrams are not applicable to this sys-

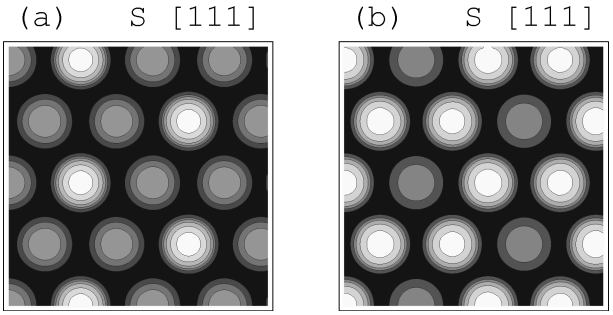

FIG. 11. Simulated TEM images of the spherical (S_{bcc}) phase at $f=0.17$, $\chi N=50$, and $\chi_{AC}/\chi=1$ viewed in the [111] direction. The contrast is proportional to $\phi_A(\mathbf{r})/2+\phi_C(\mathbf{r})$, and the sample thickness T is half the repeat distance ($T/aN^{1/2}=1.49$). The only difference between (a) and (b) is the location of the slice relative to the unit cell. Each image is $3D\times 3D$ in size, where $D/aN^{1/2}=1.72$.

tem. However, based on calculations by Zheng and Wang,[17] and the fact the experimental TEM imagines show no indication that the minority domains are continuous, we suspect Ref. 51 observed the S_{bcc} structure. Figure 11 shows some simulated TEM images of the S_{bcc} phase from the [111] direction, and indeed they agree well with the experimental images. SAXS measurements would be necessary to confirm this, but regardless it is unlikely that Ref. 51 observed a tricontinuous structure of any type.

VI. DISCUSSION

The phase behavior of ABC triblocks can be explained in terms of interfacial tension between the microdomains and the entropic stretching energy of the individual blocks, just like in the AB diblock system.[1,2] First of all, the competition between interfacial tension and coil stretching dictates the domain size D^*. This produces the usual scaling, $D^*\sim a\chi^{1/6}N^{2/3}$, at strong segregations with exponents that increase slowly as the segregation is reduced. Second, the interface develops a spontaneous curvature in an attempt to balance the stretching energy between the endblocks and the midblock. At $f\sim 1/4$ it is zero, and thus the lamellar phase is favored. As f decreases, the spontaneous curvature causes the A and C domains to evolve from lamellae, to cylinders, to spheres. Between the lamellae and cylinders, numerous complex structures possess appropriate interfacial curvatures and thus compete for stability. Third, decisions regarding how the spherical and cylindrical units pack and which complex structure is selected are subtle issues largely determined by two additional considerations.[1,2] The melt prefers a structure in which domains are uniform in thickness so as to prevent packing frustration and in which the interfacial curvature is nearly constant so as to minimize interfacial area. This favors the body-centered cubic arrangement of spheres and the hexagonal arrangement of cylinders.[34] In a moment, we will discuss why cylinders do not pack hexagonally in the ABC triblock system. Among the complex phases, gyroid is selected because it is best able to simultaneously produce uniform domains and uniform interfacial curvature.

As we have explained, it is no accident that the sequence of phases, disordered $\rightarrow S_{bcc}\rightarrow C_t\rightarrow G\rightarrow L$, in the ABC triblock system is analogous to that in the AB diblock system. The small differences that do exist can be attributed to the triblock melt having two incompatible minority domains. Because the B blocks bridge between A and C domains, it is important to place the A and C domains close together. This is satisfied by the lamellar phase and also by the gyroid phase, since it has two separate interweaving minority domains. However, the cylinder phase is forced to select a tetragonal packing, in order to interdigitate the A and C domains. The body-centered cubic packing of spheres allows a CsCl-type arrangement where all nearest-neighbor pairs have opposite compositions, and thus it remains stable in the triblock system. The inability of the A and C spherical domains to efficiently interdigitate in a fcc or hcp lattice will presumably prevent a close-packed spherical phase near the ODT, where it is predicted in the diblock system.[8,9]

In Fig. 8, it is interesting to compare the phase boundaries at $\chi_{AC}/\chi\approx 1$ for a typical ABC triblock to those at $\chi_{AC}/\chi=0$ for an ABA triblock. Because the B blocks are prevented from forming looped configurations in the ABC system, their average stretching energy is elevated. This effect is evident in Eq. (18) for the lamellar phase, and is general to all microstructures. In order to distribute some of this stretching energy to the A and C domains, the phase boundaries in the ABC triblock system are generally shifted to larger f relative to those of the ABA triblock system. One clear exception is the cylinder/gyroid transition, and this is a consequence of the cylinders reordering from hexagonal to tetragonal when the endblocks segregate. The tetragonal packing, which is necessary for alternating the A and C domains, does not fill space well and therefore causes significant packing frustration. As a result, the cylinder region is substantially reduced, and this, in turn, enlarges the complex phase region. If the frustration in C_t was sufficient, the G phase would extend to the strong-segregation limit.[1,2] However, SST calculations by Phan and Fredrickson[25] suggest that G terminates at finite χN just as it does in the AB system.[8] The additional packing frustration in C_t is also responsible for the small interval in Fig. 4 where D is more stable than L and C_t, but presumably this interval terminates around $\chi N\sim 100$ (see Sec. IV).

We have not examined the large f regime, but we can predict the behavior based on our understanding of block copolymer melts,[1,2] experiments,[15] and previous theoretical calculations.[15,17] The incompatibility of A and C blocks leads to an A/C lamellar matrix[40] with the B domains constrained to the flat A/C interfaces. This constraint on the B domains will prevent the gyroid phase from forming; the natural alternative is to form a perforated-lamellar phase. Cylindrical and spherical B domains have no problem forming at a flat interface, but it is still debatable how these units will be arranged. We expect arrays of parallel cylinders and hexagonal spheres that are staggered between adjacent interfaces. As $f\rightarrow 1/2$, the B blocks will eventually become too short to segregate into spherical domains. Entropy will cause them to spread out uniformly along the A/B interface, resulting in a

lamellar phase. In this way, the ABC triblock behavior matches up with the diblock behavior as $f \to 1/2$, which is a limit not properly treated by strong-segregation theories.[15,17] Unlike the phases examined in our study, these have A/C interfaces and so they are strongly influenced by χ_{AC}/χ. In the experiments of Mogi *et al.*,[20–23] they are apparently suppressed by the large value of χ_{AC}/χ.

The fact that ABC triblock morphologies are generally more complicated than AB diblock ones makes the self-consistent field theory (SCFT) less effective. The lower symmetry (i.e., $I4_132$ as opposed to Ia3d for the G phase) means that more basis functions are generally required to represent spatially dependent quantities at comparable degrees of segregation. Nevertheless, SCFT remains a viable method of evaluating the relative stability of complex phases. In fact, it is particularly important to use an accurate theory such as SCFT for ABC triblock melts, because many of the traditional approximations used for diblock melts are no longer legitimate. For example, the common unit-cell approximations[36] are not justified since they ignore packing frustration, which is now important even in the cylinder phase. Furthermore, the interfaces are generally more complicated, which represents a serious handicap for theories requiring the shape to be provided. Unfortunately, we cannot assume that the mean curvature of the interface is approximately constant,[52] now that we know this is not true.[1,2,53] Another difficulty is that ABC triblock morphologies often exhibit a combination of weakly and strongly segregated domains, due to, for example, a mixture of small and large blocks or unbalanced interaction parameters. The latter example occurs in Fig. 8 near the L/L′, G/G′, C_t/C_h', and S_{bcc}/S_{bcc}' transitions. In these cases, neither weak- nor strong-segregation theories will be appropriate.

VII. SUMMARY

We have examined symmetric ABC linear triblocks, where the endblocks both have a volume fraction f and the A/B and B/C interaction parameters are both χ. In this reduced parameter space, ABC triblock melts behave much like the simpler AB diblock melts because the physics involved is very similar. The competition between interfacial tension and entropic stretching energy sets the domain size. When f deviates from $\sim 1/4$, a stretching energy mismatch between the endblocks and midblock produces a spontaneous interfacial curvature that causes the minority domains to evolve from lamellae, to cylinders, to spheres. Between the lamellar and cylindrical phases, various complex phases possess appropriate interfacial curvatures, but the gyroid phase is favored because it produces the least amount of packing frustration.[1,2]

The ABC triblock system does exhibit some new behavior due to the incompatibility of the endblocks. When the endblocks form the minority domains ($f \lesssim 1/4$), there is a strong tendency for the A and C domains to alternate, because the B blocks have to bridge between them. As a result, the spherical phase only exhibits the body-centered cubic packing of minority domains, and the cylindrical phase is forced to adopt a tetragonal packing. For the cylinder phase, this produces a high degree of packing frustration that reduces its stability, enhancing the gyroid region. When the endblocks are large ($f \gtrsim 1/4$), they form an A/C lamellar matrix, confining the minority B domains to the A/C interfaces.[15,17,40] This constraint will prevent the gyroid phase and may result in a stable perforated-lamellar phase.

There is compelling evidence that the complex phase observed by Mogi *et al.*[20–22] was gyroid rather than double-diamond. First of all, only the simulated gyroid images match all the experimental TEM images (see Figs. 9 and 10). Definitive proof for gyroid appears impossible because their SAXS patterns seem unable to identify the space-group symmetry. Nevertheless, we can draw strong analogies with the diblock system for which the gyroid phase is well established.[5–7] Furthermore, the gyroid phase has been identified in an even more analogous system of symmetric ABA triblocks.[49,50] Finally, we have the fact that SCFT, a theory that has proven highly reliable, predicts gyroid to be far more stable than double-diamond. Given all this, we can still conclude with reasonable confidence that the reported double-diamond structure was a misidentified gyroid morphology.[7] Other TEM evidence for double-diamond by Matsushita *et al.*[51] can easily be attributed to a spherical phase.

We have just scratched the surface of ABC triblock behavior. Although the full parameter space for ABC triblocks is very large, we believe that a complete understanding of its phase behavior is achievable provided researchers work to extend the physical explanations developed so far. Such studies are certain to produce new and interesting behavior, and to advance our general understanding of molecular self-assembly.

Note added in proof. We have been informed that Matsushita *et al.*[54] have independently presented evidence that the complex phase in Refs. 20–22 is gyroid.

ACKNOWLEDGMENTS

We are grateful to F. S. Bates for motivating this study, and to D. A. Hajduk for sharing his expertise in SAXS. We also thank S. Phan and G. H. Fredrickson for supplying us with a copy of their manuscript prior to publication.

[1] M. W. Matsen and F. S. Bates, J. Chem. Phys. **106**, 2436 (1997).
[2] M. W. Matsen and F. S. Bates, Macromolecules **29**, 7641 (1996).
[3] F. S. Bates and G. H. Fredrickson, Annu. Rev. Phys. Chem. **41**, 525 (1990); F. S. Bates, F. S. Schulz, A. K. Khandpur, S. Förster, J. H. Rosedale, K. Almdal, and K. Mortensen, Faraday Discuss. **98**, 7 (1994).
[4] M. W. Matsen and F. S. Bates, J. Polym. Sci. Part B **35**, 945 (1997).
[5] D. A. Hajduk, H. Takenouchi, M. A. Hillmyer, F. S. Bates, M. E. Vigild, and K. Almdal, Macromolecules **30**, 3788 (1997).
[6] M. F. Schulz, F. S. Bates, K. Almdal, and K. Mortensen, Phys. Rev. Lett. **73**, 86 (1994); D. A. Hajduk, P. E. Harper, S. M. Gruner, C. C. Honeker, G. Kim, E. L. Thomas, and L. J. Fetters, Macromolecules **227**, 4063 (1994).
[7] D. A. Hajduk, P. E. Harper, S. M. Gruner, C. C. Honeker, E. L. Thomas, and L. J. Fetters, Macromolecules **28**, 2570 (1995).
[8] M. W. Matsen and F. S. Bates, Macromolecules **29**, 1091 (1996).
[9] A. N. Semenov, Macromolecules **22**, 2849 (1989).
[10] N. Sakamoto, T. Hashimoto, C. D. Han, D. Kim, and N. Y. Vaidya, Macromolecules **30**, 1621 (1997).
[11] S. L. Aggarwal, Polymer **17**, 938 (1976).

[12] E. L. Thomas, D. B. Alward, D. J. Kinning, D. C. Martin, D. L. Handlin, and L. J. Fetters, Macromolecules **19**, 2197 (1986).
[13] M. W. Matsen and M. Schick, Macromolecules **27**, 6761 (1994); **27**, 7157 (1994).
[14] M. W. Matsen, J. Chem. Phys. **102**, 3884 (1995); R. L. Lescanec, D. A. Hajduk, G. Y. Kim, Y. Gan, R. Yin, S. M. Gruner, T. E. Hofen-Esch, and E. L. Thomas, Macromolecules **28**, 3485 (1995).
[15] R. Stadler, C. Auschra, J. Beckmann, U. Krappe, I. Voigt-Martin, and L. Leibler, Macromolecules **28**, 3080 (1995).
[16] C. Auschra and R. Stadler, Macromolecules **26**, 2171 (1993); U. Krappe, R. Stadler, and I. Voight-Martin, *ibid.* **28**, 4558 (1995); B. Ulrike, K. Udo, and R. Stadler, Macromol. Rapid Commun. **17**, 567 (1996).
[17] W. Zheng and Z.-G. Wang, Macromolecules **28**, 7215 (1995).
[18] T. Ohta and K. Kawasaki, Macromolecules **19**, 2621 (1986).
[19] H. Nakazawa and T. Ohta, Macromolecules **26**, 5503 (1993).
[20] Y. Mogi, H. Kotsuji, Y. Kaneko, K. Mori, Y. Matsusita, and I. Noda, Macromolecules **25**, 5408 (1992).
[21] Y. Mogi, K. Mori, Y. Matsushita, and I. Noda, Macromolecules **25**, 5412 (1992).
[22] Y. Mogi, M. Nomura, H. Kotsuji, K. Ohnishi, Y. Matsushita, and I. Noda, Macromolecules **27**, 6755 (1994).
[23] Y. Mogi, K. Mori, H. Kotsuji, Y. Matsushita, I. Noda, and C. C. Han, Macromolecules **26**, 5169 (1993).
[24] T. Dotera and A. Hatano, J. Chem. Phys. **105**, 8413 (1996).
[25] S. Phan and G. H. Fredrickson, Macromolecules (submitted).
[26] A. N. Semenov, Sov. Phys. JETP **61**, 733 (1985).
[27] E. Helfand, J. Chem. Phys. **62**, 999 (1975); Macromolecules **8**, 552 (1975).
[28] M. W. Matsen and M. Schick, Phys. Rev. Lett. **72**, 2660 (1994).
[29] The unnormalized basis functions can be found in *International Tables for X-Ray Crystallography*, edited by N. F. M. Henry and K. Lonsdale (Kynoch, Birmingham, 1969). The two-dimensional space-group symmetries of the C_t and C_h' phases are numbers 11 and 17, respectively. The three-dimensional ones of the S_{bcc}, S_{bcc}', S_{cp}', G, G′, D, and D′ phases are 221, 229, 194, 214, 230, 227, and 224, respectively.
[30] We solve the self-consistent field equations using the Broyden algorithm. See R. L. Burden, J. D. Faires, and A. C. Reynolds, *Numerical Analysis*, 2nd ed. (PWS, Boston, 1981), p. 458.
[31] L. Leibler, Macromolecules **13**, 1602 (1980).
[32] M. W. Matsen and F. S. Bates, Macromolecules **28**, 8884 (1995).
[33] L. Kane and R. J. Spontak, Macromolecules **27**, 1267 (1994).
[34] E. L. Thomas, D. J. Kinning, D. B. Alward, and C.S. Henkee, Macromolecules **20**, 2934 (1987).
[35] C. Neumann, V. Abetz, and R. Stadler, Polym. Bull. **36**, 43 (1996).
[36] M. W. Matsen and M. D. Whitmore, J. Chem. Phys. **105**, 9698 (1996).
[37] E. Helfand and Z. R. Wasserman, Macromolecules **9**, 879 (1976).
[38] J. L. Goveas, S. T. Milner, and W. B. Russel, Macromolecules **30**, 5541 (1997).
[39] Yu. V. Lyatskaya and T. M. Birshtein, Polymer **36**, 975 (1995).
[40] In the large *f* limit, Stadler *et al.* (Ref. 15) predict a matrix of A cylinders in C and vice versa. We attribute this nonintuitive result, which contradicts calculations by Zheng and Wang,[17] to inaccurate approximations.
[41] A. E. Likhtman and A. N. Semenov, Macromolecules **27**, 3103 (1994); P.D. Olmsted and S. T. Milner, Phys. Rev. Lett. **72**, 936 (1994); *ibid.* **74**, 829 (1995).
[42] A. E. Likhtman and A. N. Semenov, Macromolecules **30**, 7273 (1997).
[43] A. Werner and G. H. Fredrickson, J. Polym. Sci. Part B **35**, 849 (1997).
[44] V. E. Podneks and I. W. Hamley, JETP Lett. **64**, 617 (1996); I. W. Hamley and V. E. Podneks, Macromolecules **30**, 3701 (1997).
[45] G. H. Fredrickson and E. Helfand, J. Chem. Phys. **87**, 697 (1987).
[46] P. M. Lipic, J. Zhao, M. W. Matsen, D. A. Hajduk, M. B. Kossuth, and F. S. Bates (in preparation).
[47] M. W. Matsen, Phys. Rev. Lett. **74**, 4225 (1995); Macromolecules **28**, 5765 (1995).
[48] Mogi *et al.* (Ref. 22) have assumed the wrong space-group for double-diamond, which allows extra reflections at [200] and [420].
[49] J. H. Laurer, D. A. Hajduk, J. C. Fung, J. W. Sedat, S. D. Smith, S. M. Gruner, D. A. Agard, and R. J. Sontak, Macromolecules **30**, 3938 (1997).
[50] A. Avgeropoulos, B. J. Dair, N. Hadjichristidis, and E. L. Thomas, Macromolecules **30**, 5634 (1997).
[51] Y. Matsushita, M. Tamura, and I. Noda, Macromolecules **27**, 3680 (1994).
[52] E. L. Thomas, D. M. Anderson, C. S. Henkee, and D. Hoffman, Nature (London) **334**, 598 (1988).
[53] S. P. Gido, D. W. Schwark, E. L. Thomas, and M. Gonçalves, Macromolecules **26**, 2636 (1993).
[54] Y. Matsushita, J. Suzuki, and M. Seki, Physica A (in press).